Mineralogy and Petrology (2021) 115:611–630
https://doi.org/10.1007/s00710-021-00757-9

ORIGINAL PAPER

Water contents of nominally anhydrous orthopyroxenes from oceanic peridotites determined by SIMS and FTIR

Kirsten T. Wenzel[1] · Michael Wiedenbeck[2] · Jürgen Gose[1] · Alexander Rocholl[2] · Esther Schmädicke[1]

Received: 12 January 2021 / Accepted: 19 July 2021 / Published online: 27 August 2021

Abstract

This study presents new secondary ion mass spectrometry (SIMS) reference materials (RMs) for measuring water contents in nominally anhydrous orthopyroxenes from upper mantle peridotites. The enstatitic reference orthopyroxenes from spinel peridotite xenoliths have Mg#s between 0.83 and 0.86, Al_2O_3 ranges between 4.02 and 5.56 wt%, and Cr_2O_3 ranges between 0.21 and 0.69 wt%. Based on Fourier-transform infrared spectroscopy (FTIR) characterizations, the water contents of the eleven reference orthopyroxenes vary from dry to 249 ± 6 µg/g H_2O. Using these reference grains, a set of orthopyroxene samples obtained from variably altered abyssal spinel peridotites from the Atlantic and Arctic Ridges as well as from the Izu-Bonin-Mariana forearc region was analyzed by SIMS and FTIR regarding their incorporation of water. The major element composition of the sample orthopyroxenes is typical of spinel peridotites from the upper mantle, characterized by Mg#s between 0.90 and 0.92, Al_2O_3 between 1.66 and 5.34 wt%, and Cr_2O_3 between 0.62 and 0.96 wt%. Water contents as measured by SIMS range from 68 ± 7 to 261 ± 11 µg/g H_2O and correlate well with Al_2O_3 contents (r = 0.80) and Cr#s (r = -0.89). We also describe in detail an optimized strategy, employing both SIMS and FTIR, for quantifying structural water in highly altered samples such as abyssal peridotite. This approach first analyzes individual oriented grains by polarized FTIR, which provides an overview of alteration. Subsequently, the same grain along with others of the same sample is measured using SIMS, thereby gaining information about homogeneity at the hand sample scale, which is key for understanding the geological history of these rocks.

Keywords FTIR · Hydrogen · Nominally anhydrous minerals · Orthopyroxene · SIMS · Spinel peridotite

Introduction

Understanding the role of water, its amount and distribution in the Earth's upper mantle and its influence on convective processes and geodynamics is a key task of igneous geochemistry. Water decreases the mantle's viscosity and mechanical strength via hydrolytic weakening of olivine (Demouchy et al. 2012; Tielke et al. 2017) and lowers peridotite melting temperatures (e.g. Hirth and Kohlstedt 1996), thereby affecting melting depth and thus the composition of the melt (Hauri et al. 2006).

Incorporated by various substitutions, such as protons attached to oxygen anions forming "hydroxyl defects" in the crystal structure (Bell and Rossman 1992; Libowitzky and Beran 2006), small amounts of water can be found in nominally anhydrous minerals (NAMs) such as pyroxenes and olivines derived from the Earth's upper mantle. Olivine is believed to dehydrate rapidly (e.g. Mackwell and Kohlstedt 1990) when decompressed during tectonic uplift or magmatic transport to the surface as recorded by core-rim zonation in natural grains (Demouchy et al. 2006; Peslier and Luhr 2006; Schmädicke et al. 2013). Although H loss has recently been observed in pyroxenes as well (Tian et al. 2016; Denis et al. 2018), orthopyroxene is generally considered to retain its upper mantle water concentration during exhumation (Gose et al. 2011; Hao et al. 2014; Azevedo-Vannson et al. 2021) and can be used as a reliable tracer for water in the upper mantle (Denis et al. 2013; Warren and

Editorial handling: A. Beran

✉ Kirsten T. Wenzel
kirsten.hesse@fau.de

[1] GeoZentrum Nordbayern, University of Erlangen-Nürnberg, Schlossgarten 5a, Erlangen 91054, Germany

[2] Deutsches GeoForschungsZentrum GFZ, Telegrafenberg, Potsdam 14473, Germany

Hauri 2014). A number of studies on experimental and natural orthopyroxene have shown that the mineral can hold up to several hundred µg/g H_2O, making it a significant reservoir for water in the upper mantle (Bell and Rossman 1992; Hirschmann et al. 2005; Peslier 2010).

Several laboratory methods are capable of quantifying hydrogen in NAMs: vacuum manometry is an easily available technique but is also destructive and requires large enough alteration-free sample volumes (Aubaud et al. 2007), which can be problematic in the case of NAMs in upper mantle rocks. Nuclear reaction analysis (NRA) and elastic recoil detection analysis (ERDA) are also reliable techniques for determining hydrogen contents in mantle minerals (Bell et al. 2003; Withers et al. 2012) but the necessary facilities are often difficult to access (Aubaud et al. 2007). More widespread spectroscopic approaches such as nuclear magnetic resonance (NMR; Rauch and Keppler 2000; Kohn 2006) are difficult to use when iron is present in the matrix (Aubaud et al. 2007). A more detailed review of the different methods is given by Rossman (2006) and recent analytical advances are also discussed in Sheng et al. (2016).

For these reasons, FTIR has long been the method of choice for investigating the hydrogen distribution in NAMs (Rossman 2006; Mosenfelder et al. 2011). In contrast to other techniques, the method itself (after sample preparation) is non-destructive and yields information about the vibrational energy and orientation of OH-dipoles in the crystal structure. It can thus distinguish structurally incorporated hydrogen from water contained in impurities such as secondary hydrous phases, alteration products or fluid inclusions (Rossman 1996; Libowitzky and Beran 2004). Numerous studies have taken advantage of this specificity to document trace amounts of structurally bound water in olivine, ortho-, and clinopyroxene from abyssal peridotites which are often overprinted by alteration (Gose et al. 2009, 2011; Peslier 2010; Schmädicke et al. 2011, 2018; Hesse et al. 2015; Gose and Schmädicke 2021). Generally, there are different approaches when using infrared spectroscopy: (i) analysis of oriented crystals using polarized radiation or (ii) analysis of unoriented crystals using unpolarized radiation (statistical method). Regarding the first method, the orthopyroxene grains in abyssal peridotites are either very small or broken into fragments, which makes it difficult to prepare oriented crystals to be analyzed by polarized radiation. For analyzing randomly oriented crystals using unpolarized radiation one would need to examine a large number of grains in order to get a statistically robust representation of the sample. In contrast to xenoliths, abyssal peridotites are often highly altered, i.e. serpentinized and exhibit a typical porphyroclastic texture, meaning there are often only two or three individual orthopyroxene grains available when preparing sections of hand samples. Even if one were able to find enough individual grains, with this method one would get the average water content for the sample with little or no information about the heterogeneity of the material. In either case, sample preparation for FTIR can be difficult and time-consuming and strongly depends on sample quality and size. Moreover, there are significant, unresolved calibration issues regarding which molar absorption coefficients are appropriate (e.g. Mosenfelder and Rossman 2013) and there is no agreed procedure as to how the data should be processed (manual versus mathematical correction of absorption baseline), which can introduce major biases between data sets obtained by different working groups.

Because of these challenges, a number of recent studies have chosen SIMS as a means to quantify H_2O contents in NAMs (e.g. Warren and Hauri 2014; Kumamoto et al. 2017). This method offers the advantage of high spatial resolution, often better than 10 µm, and insensitivity to crystal orientation (Koga et al. 2003). The main drawback of SIMS is that it detects the bulk hydrogen content of a material, meaning it cannot distinguish between different water species. This, however, is important in the case of abyssal peridotites which commonly contain secondary hydrous phases. Moreover, SIMS cannot directly determine elemental concentrations - it can only compare the secondary ion signal from well-characterized reference to that from an "unknown" sample. Crucially, such SIMS RMs must be closely matrix-matched to the actual samples being tested. Thus, for SIMS one needs to first establish a calibration curve, preferably based on multiple, well-characterized RMs. Only once this has been achieved can meaningful analyses of actual samples be undertaken.

The aims of this study are to (i) identify reference orthopyroxene crystals that are well suited for calibrating SIMS, (ii) quantify H_2O concentrations in natural orthopyroxene samples using this calibration, (iii) compare our SIMS results to the results obtained independently by FTIR, and (iv) evaluate the methods in order to establish a robust methodology for determining intra-crystalline water contents in orthopyroxene recovered from abyssal peridotites (harzburgites), even when such material may have experienced extensive serpentinization.

Materials and preparation

Orthopyroxene reference materials

Eight orthopyroxenes from spinel peridotites occurring as xenoliths in alkali basalts from Western Mongolia (hand samples Mo21, Mo22, and Mo8531) and three orthopyroxenes from spinel peridotites from the Eifel volcanic field in Western Germany (hand samples E-K1 and 1b-5) were selected for characterization as reference minerals. These peridotites consist of the four-phase assemblage olivine,

orthopyroxene, clinopyroxene, and spinel. For further details see Schmädicke et al. (2013) on samples from Western Mongolia and E-K1 and Stosch and Seck (1980) for sample 1b-5. The eleven, up to 3 mm sized orthopyroxene grains that were selected for use as RMs were optically clear and free of fractures.

Orthopyroxene samples from abyssal peridotites

The twelve samples to be analyzed by SIMS include orthopyroxenes recovered from abyssal spinel peridotites (harzburgites) from various locations along the Mid-Atlantic Ridge (MAR), the Gakkel Ridge, Arctic Ocean, and the Izu-Bonin-Mariana forearc region (IBM; Table 1). The samples were recovered by either drilling (DSDP and ODP samples) or dredging and diving expeditions. Where large enough hand samples were available, thin sections were made on which the degree of serpentinization was assessed qualitatively (Fig. 1).

The rocks are moderately to highly altered. The primary mineral assemblage consists of olivine (ol), orthopyroxene (opx), brown spinel (spl), and minor clinopyroxene (cpx). In some samples olivine has been entirely replaced by serpentine, whereas in other samples fresh olivine kernels are preserved in the centers of concentric layers of serpentine ("mesh texture"). Orthopyroxene invariably forms up to mm-sized crystals, heavily broken into fragments, which are partially preserved (porphyroclastic texture). Most of the preserved orthopyroxene fragments contain amphibole lamellae, others are entirely altered or replaced by bastite. Primary clinopyroxene is rare to absent in these samples. Spinel grains formed interstitially, leading to highly irregular shapes. For further information on the petrology of the samples, see Regelous et al. (2016).

Sample preparation

For the FTIR analyses, the peridotite reference orthopyroxenes were cut out of the hand samples using a saw. Xenoliths were slightly crushed and easily disaggregated thanks to their less compact structure. The RM grains were then prepared as cuboid bodies and polished on all six planar sides. The thickness of the cuboids was measured with a precision of ≤3 µm using an electronic micrometer and varied between 516 and 1746 µm.

Since the abyssal peridotite samples are highly altered and the orthopyroxene grains are commonly fragmented, few crystals suitable for FTIR analysis could optically be identified in the hand rock samples and thin sections. We therefore proceeded to crush (instead of sawing) selected rock portions. Because of their greater mechanical strength, the peridotite samples required crushing with severe force. Suitable orthopyroxene grain fragments, optically clear and without visible fractures, inclusions, and alteration products were hand-picked under a binocular microscope, individually embedded in epoxy, grinded down and polished on two sides. For the final polishing step a 3 µm diamond paste was used. This way, numerous orthopyroxene fragments from all samples could be prepared for FTIR analysis. The measurements were performed in three sessions in three randomly oriented but orthogonal planes. Sample thicknesses varied between 80 and 812 µm.

Upon having determined all water contents via FTIR, the RM Mo22-opx3 was dehydrated in a furnace at 1000 °C in air for 24 hours such that the grain could be used as a blank to determine the level of hydrogen background during the subsequent SIMS analyses. Dehydration was verified by FTIR according to the analytical procedure described below.

After completion of the FTIR analyses, pieces of the eleven reference grains were embedded in Epo-Tek® 301

Table 1 Summary of abyssal peridotites investigated in this study

Sample	Lithology	Location	Degree of alteration
ODP304-1309B-11R-1W ODP304-1309B-11R-2W	Serpentinite with opx and ol relics	30°N, Mid-Atlantic Ridge (Atlantis Massif)	very high
DSDP45-395-18R-1W-112	Serpentinized harzburgite	23°N, Mid-Atlantic Ridge	moderate
PS59-249-Br4	n.a.	Gakkel Ridge	n.a.
ODP109-670A-4R-1W	Serpentinized harzburgite	23°N, Mid-Atlantic Ridge	high
HLY-102-D32	n.a	Gakkel Ridge	n.a.
ODP125-0779A-26R-2W	Serpentinized harzburgite	Izu-Bonin-Mariana forearc region (Conical Seamount)	n.a.
PS55-75-30	Serpentinized harzburgite	Arctic Ocean (Fram Strait)	high
ODP209-1272A-26R-1W-60-65	Serpentinized harzburgite	15°N, Mid-Atlantic Ridge	n.a.
PS59-236-80-500-900	n.a.	Gakkel Ridge	n.a.
ME41/2-KD5-1	Serpentinite with opx relics	Southern Atlantic Ocean	very high

n.a. indicates that no thin section was available for the respective sample

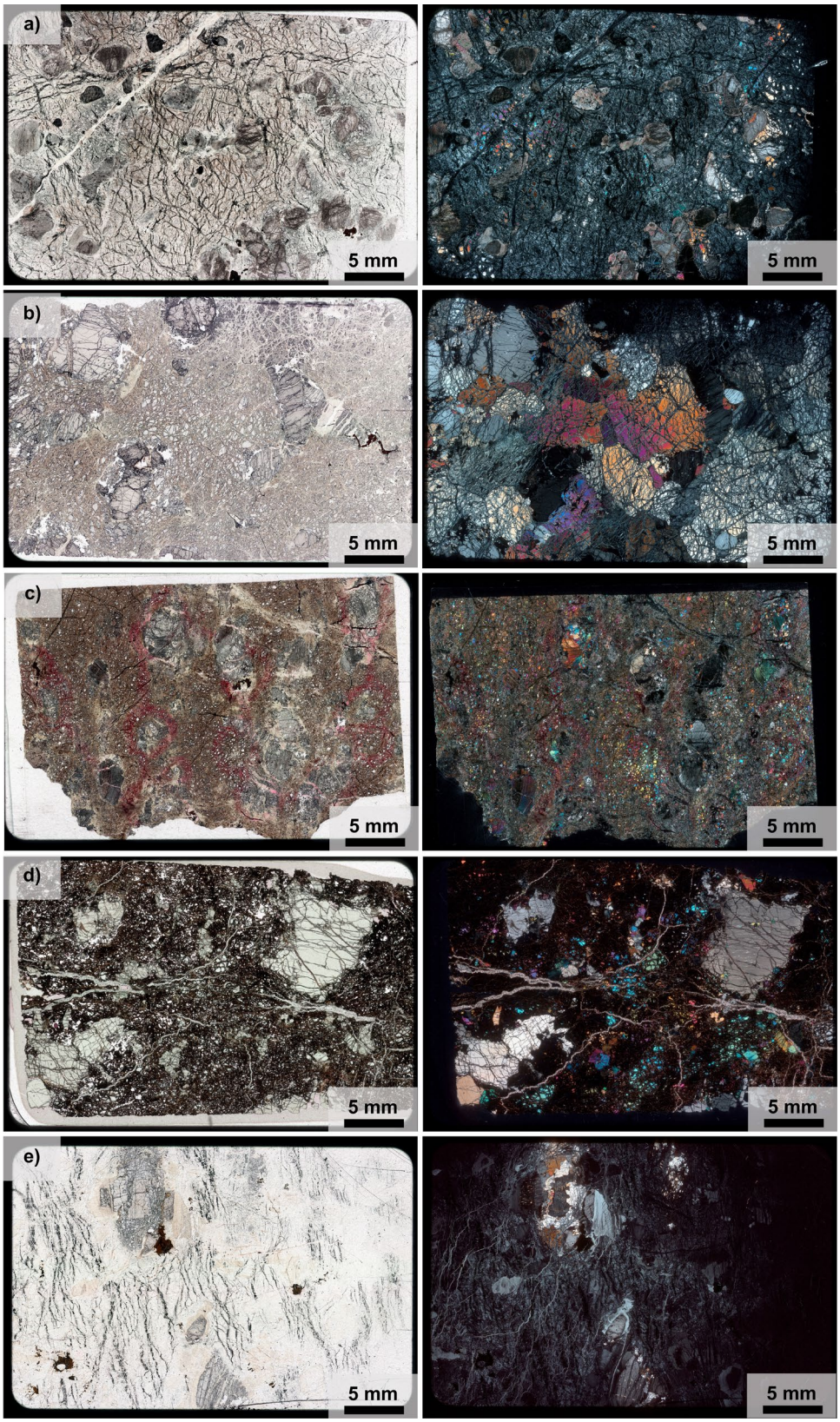

Fig. 1 Plane-polarized (left) and cross-polarized (right) transmitted-light photomicrographs of thin sections from selected variably altered abyssal peridotite samples: **a**) ODP304 (IBM), **b**) DSDP45 (MAR), **c**) ODP109 (MAR), **d**) PS55-75 (Arctic Ocean), **e**) ME41/2 (Southern Atlantic Ocean)

(Epoxy Technology epoxy resin) and prepared as a 1-inch diameter round mount, which was polished and carbon-coated for the EPMA (electron probe micro-analyzer) analyses. This mount was also used for the calibration of the hydrogen quantification by SIMS. Prior to the SIMS analyses, the carbon coating was taken off, the mount was washed in distilled water, followed by ultrasonic cleaning in high-purity ethanol followed by argon sputter coating to produce a 35 nm thick, high-purity conductive gold film across the sample surface. It was then loaded into the sample holder and stored in the SIMS' high vacuum airlock for 72 hours.

Since sample outgassing became a problem, the reference grains were removed from the epoxy, cleaned and recast in indium metal using a hand press. Unfortunately, during this process, two of the reference grains (Mo22-opx6 and E-K1-opx3) were lost. The new indium mount was washed, cleaned and gold-coated as described above. For analyzing the hydrogen contents of the abyssal peridotite orthopyroxene samples, these grains together with three RMs (Mo21-opx1, Mo22-opx5, and 1b-5-opx1) were embedded in a second indium mount following the same procedure.

Major elements of the orthopyroxene samples were analyzed on this second indium mount after the SIMS session. Therefore, the gold coating was taken off by polishing the mount by hand with 1 µm diamond paste. Afterwards, the mount was cleaned and sputtered with carbon.

Analytical methods

EPMA analysis

All major-element analyses were performed using a JEOL JXA-8200 electron microprobe equipped with five wavelength dispersive spectrometers. The analyses were run at a 15 kV acceleration voltage and a 15 nA probe current. A ~5 µm beam diameter was used for Na, whereas a <1 µm diameter was used for all other elements. Peak and background counting times were 20 s each. The following natural and synthetic materials were used for calibration: Al_2O_3 (Al), wollastonite (Ca, Si), Cr_2O_3 (Cr), Fe_2O_3 (Fe), MgO (Mg), $MnSiO_3$ (Mn), albite (Na), NiO (Ni), rutile (Ti), and sphalerite (Zn). Kα lines were analyzed for all elements. The data were corrected using an iterative ZAF algorithm. Dispersed between samples a diopside crystal with known composition was analyzed both as a quality control material and for checking instrumental drift. The relative analytical uncertainties are approximately 1 % for elemental concentrations above 2 wt%, whereas relative uncertainties of ~5 % are estimated for element abundances below 2 wt%.

Eight analyses per grain were performed on the reference orthopyroxenes to check for compositional zoning. Element maps including the major elements Ti, Mg, Mn, Fe, Ca, Al, Cr, and Ni were recorded for assessing chemical homogeneity. For the calculation of mineral formulae, all iron was treated as ferrous iron (Fe^{2+}).

FTIR spectroscopy

A Bruker Vertex 70 FTIR spectrometer, equipped with a KBr beam splitter and coupled to a Hyperion 3000 microscope with an MCT detector was used for all FTIR analyses in this study. The measurements were performed in three randomly oriented but orthogonal planes of the prepared crystals with perpendicular polarizer positions parallel to minimum and maximum absorption according to the method of Libowitzky & Rossman (1996). The RMs and samples were analyzed with a spectral resolution of 2 cm^{-1} across the 7500-550 cm^{-1} wavenumber range. At least 64 scans were acquired for each spectrum. Rectangular apertures between 80x100 μm^2 and 150x150 μm^2 were used to define the analyzed area in the case of the reference orthopyroxenes. For the unknown samples, apertures between 30x30 and 80x80 μm^2 depending on crystal quality were used. Special care was taken to solely analyze optically clear and inclusion- and alteration-free spots. For internal comparison, three different spots were analyzed per grain, each containing a set of six spectra. A background correction for atmospheric H_2O and CO_2 was applied following each measurement.

Water concentrations (in µg/g H_2O) were derived from the integral absorbance normalized to 1 cm thickness applying the mineral-specific molar absorption coefficient from Bell et al. (1995). For baseline correction, a third degree polynomial function was utilized to subtract the background between 3700 and 2800 cm^{-1}. The analytical uncertainties for spectra with small interferences from amphibole bands in the same wavenumber range as the observed orthopyroxene bands are estimated to amount to 10–15%. Upon request, extensive data can be obtained from the corresponding author.

Secondary ion mass spectrometry

SIMS calibration

Determinations of H_2O contents by SIMS were conducted using a Cameca 1280-HR instrument. The first series of analyses of the reference orthopyroxene crystals used a mass filtered $^{133}Cs^+$ primary ion beam with a total impact energy of 20 keV. $^{16}O^1H^-$ ions were measured as a proxy for the hydrogen content as this molecule provided more stable within-run data than did $^1H^-$. Despite the SIMS' high-vacuum conditions of 5×10^{-7} Pa in the sample chamber, we were unable to produce consistent $^{16}O^1H^-/^{18}O^-$ ratios. Even the most hydrogen enriched RM (1b-5-opx1, 249 ± 6 µg/g H_2O according to FTIR) was affected by hydrogen

adsorption onto the sample surface at the point of analysis during data acquisition. Much of this background could be attributed to electron-induced desorption of OH that resulted from the need to use low energy electron flooding when operating in negative secondary ion polarity.

Therefore, an alternative analytical set-up was tested using a duoplasmatron to generate $^{16}O^-$ as primary ions and recording the $^{28}Si^1H^+/^{29}Si^+$ ion ratio. This alternative approach provided no advantages and was further complicated by an unstable primary ion current that dropped from roughly 2.0 nA to 0.8 nA during the analytical session. This resulted in an increase in the observed $^{28}Si^1H^+/^{29}Si^+$ measured ratio as one would expect when hydrogen was mostly coming from vacuum contamination adsorbed during the analysis. We therefore decided it was necessary to remove all crystals from the epoxy and recast them in indium.

For the next series of analyses, the $^{16}O^-$ primary current was increased to 30 nA, the field of view was reduced to only 10 µm by closing the field aperture, and the primary beam raster was turned off. Furthermore, the positioning of external permanent magnets was adjusted such that H could be run as an ion rather than a molecule. A long duration liquid nitrogen cold trap was used during the run to improve the vacuum (1.2×10^{-7} Pa). Limit of detection under these conditions was around 5 to 10 µg/g H_2O. This new approach, however, required a spot size of over 30 µm.

Analyses of abyssal peridotite orthopyroxene samples

For analyzing the hydrogen contents of the abyssal peridotite orthopyroxene samples, the SIMS determinations employed a $^{16}O^-$ primary ion beam operating with a 30 nA current with a total impact energy of 23 keV in Gaussian mode, providing a *circa* 25 µm diameter beam at the point of impact on the polished sample surface. Each analysis was preceded by a 90 s pre-sputtering using a 50×50 µm^2 raster. Prior to taking data, the raster was turned off. In order to assure that the crater was precisely centered on the field aperture, a centering scan was conducted prior to each analysis using two sets of orthogonal electrical deflection plates. To avoid hydrogen adsorbed from the residual glasses in the analysis chamber (total pressure range from 2.7 to 2.3×10^{-7} Pa) a small field aperture of 550×550 µm^2 was used, equivalent of a field of view of only 6×6 µm^2. Thus, the field of view of the mass spectrometer was limited to the very center of the primary beam's Gaussian distribution. The mass spectrometer was operated in dynamic mono-collection mode at a mass resolution of $M/\Delta M \approx 2500$ at 10 % peak height. A 150 eV wide energy bandpass was used. A single analysis consisted of 16 cycles of peak switching between ^1H (4 seconds per cycle) and ^{30}Si (1 s), thus a single analysis required a little over three minutes including the pre-sputtering process. All data were recorded using an ETP133H pulse counter to which deadtime correction of 46.2 ns was applied based on a delay circuit in the pre-amplifier electronics. The $^1H/^{30}Si$ repeatability on n = 13 determinations spread over the two-day analytical session on our most hydrogen enriched reference material (1b-5-opx1, 249 ± 6 µg/g H_2O) was ± 3.2 % (1s). The best-fit regression line for the n = 41 analyses conducted in total on the three RMs yielded $R^2 = 0.90$, so we infer that a linear calibration between $[H_{(\mu g/g)}/SiO_{2(wt\%)}]_{true}$ vs. $[^1H^+/^{30}Si^+]_{measured}$ is reasonable. However, this regression line had a negative intercept value, equivalent to -8 µg/g H_2O. Since the vacuum conditions during this run were comparable to those during the calibration of the mount containing the blank, we conclude that the H_2O background for these analyses was comparably low, probably in the single digit µg/g range, and therefore decided to use a linear fit forcing the calibration line through zero for the calculation of the H_2O contents of the samples. We have thus not applied any further background correction, but one must bear in mind that for samples with lower hydrogen contents there may be a few µg/g background which has not been addressed and that such SIMS data might have a small systematic offset.

Results

Reference orthopyroxene

Major element compositions

The multiple analyses per grain do not vary significantly, confirming good homogeneity for our suite of RMs. All orthopyroxene grains are enstatitic with Mg#s, defined as MgO/(MgO+FeO), between 0.83 and 0.86 and Cr#s, defined as $Cr_2O_3/(Cr_2O_3+Al_2O_3)$, between 0.05 and 0.12. Mean MgO ranges from 31.4 ± 0.2 wt% (Mo22-opx2) to 32.9 ± 0.2 wt% (Mo8531-opx1), mean FeO from 5.30 ± 0.16 wt% (E-K1-opx1) to 6.58 ± 0.13 wt% (Mo21-opx1). Mean SiO_2 varies between 53.9 ± 0.3 wt% (1b-5-opx1) and 55.1 ± 0.2 wt% (Mo8531-opx1), mean Al_2O_3 between 4.02 ± 0.06 wt% (Mo8531-opx1) and 5.56 ± 0.06 wt% (E-K1-opx1), and mean Cr_2O_3 between 0.21 ± 0.04 wt% (Mo21-opx2) and 0.69 ± 0.02 wt% (1b-5-opx1) (Table 2).

FTIR spectra and water contents

The FTIR spectra of orthopyroxenes Mo21-opx1, Mo22-opx5, and 1b-5-opx1, which were used as RMs for the SIMS analyses of the samples, are shown in Fig. 2a-c. These spectra were recorded at three different locations on each grain (1, 2, 3) using both horizontal (h) and vertical (v) polarization (parallel to the minimum and maximum absorption) in three random but mutually orthogonal directions (A, B, C),

Table 2 Averaged major element compositions of the reference orthopyroxenes measured by EPMA

Reference orthopyroxene	SiO_2 [wt%]	TiO_2 [wt%]	Al_2O_3 [wt%]	Cr_2O_3 [wt%]	FeO[a] [wt%]	MnO [wt%]	MgO [wt%]	NiO [wt%]	ZnO [wt%]	CaO [wt%]	Na_2O [wt%]	Total [wt%]	Mg#[b]	Cr#[c]	N
Mo21-opx1*	54.90 ± 0.14	0.16 ± 0.01	4.63 ± 0.10	0.27 ± 0.03	6.58 ± 0.13	0.17 ± 0.03	32.44 ± 0.19	0.10 ± 0.02	0.01 ± 0.02	0.46 ± 0.06	0.10 ± 0.01	99.80 ± 0.36	0.83 ± 0.00	0.06 ± 0.01	8
Mo21-opx2	54.95 ± 0.35	0.15 ± 0.02	4.38 ± 0.23	0.21 ± 0.04	6.53 ± 0.14	0.15 ± 0.03	32.79 ± 0.12	0.08 ± 0.03	0.02 ± 0.03	0.42 ± 0.03	0.09 ± 0.01	99.78 ± 0.33	0.83 ± 0.00	0.05 ± 0.01	8
Mo22-opx1	54.35 ± 0.40	0.15 ± 0.02	5.02 ± 0.07	0.35 ± 0.03	6.23 ± 0.13	0.13 ± 0.03	32.02 ± 0.13	0.11 ± 0.02	0.03 ± 0.02	0.83 ± 0.04	0.19 ± 0.02	99.40 ± 0.52	0.84 ± 0.00	0.06 ± 0.01	8
Mo22-opx2	54.2 ± 0.34	0.17 ± 0.02	5.34 ± 0.12	0.39 ± 0.02	6.27 ± 0.06	0.15 ± 0.01	31.42 ± 0.20	0.10 ± 0.03	0.03 ± 0.03	0.89 ± 0.04	0.21 ± 0.01	99.16 ± 0.43	0.83 ± 0.00	0.07 ± 0.00	8
Mo22-opx3	54.6 ± 0.28	0.17 ± 0.02	5.05 ± 0.09	0.34 ± 0.02	6.20 ± 0.16	0.14 ± 0.01	32.04 ± 0.28	0.11 ± 0.02	0.01 ± 0.02	0.87 ± 0.03	0.20 ± 0.02	99.80 ± 0.57	0.84 ± 0.00	0.06 ± 0.00	8
Mo22-opx4	54.4 ± 0.22	0.15 ± 0.02	5.19 ± 0.11	0.37 ± 0.04	6.29 ± 0.06	0.17 ± 0.02	31.96 ± 0.22	0.11 ± 0.02	0.02 ± 0.03	0.87 ± 0.02	0.18 ± 0.02	99.79 ± 0.33	0.84 ± 0.00	0.07 ± 0.01	8
Mo22-opx5*	54.52 ± 0.22	0.17 ± 0.02	5.19 ± 0.08	0.37 ± 0.03	6.28 ± 0.09	0.15 ± 0.01	31.86 ± 0.19	0.09 ± 0.03	0.01 ± 0.02	0.88 ± 0.03	0.19 ± 0.02	99.71 ± 0.41	0.84 ± 0.00	0.07 ± 0.01	8
Mo22-opx6	54.51 ± 0.16	0.16 ± 0.02	5.21 ± 0.11	0.37 ± 0.02	6.30 ± 0.15	0.16 ± 0.03	31.99 ± 0.09	0.12 ± 0.03	0.03 ± 0.03	0.91 ± 0.01	0.19 ± 0.00	99.94 ± 0.29	0.84 ± 0.00	0.07 ± 0.00	8
Mo8531-opx1	55.09 ± 0.16	0.17 ± 0.02	4.02 ± 0.06	0.28 ± 0.03	5.91 ± 0.09	0.14 ± 0.01	32.93 ± 0.21	0.08 ± 0.02	0.01 ± 0.01	0.46 ± 0.03	0.07 ± 0.02	99.17 ± 0.39	0.85 ± 0.00	0.06 ± 0.01	6
E-K1-opx1	54.20 ± 0.20	0.17 ± 0.03	5.56 ± 0.06	0.63 ± 0.02	5.30 ± 0.16	0.13 ± 0.01	31.89 ± 0.19	0.09 ± 0.03	0.03 ± 0.03	1.17 ± 0.03	0.19 ± 0.02	99.36 ± 0.39	0.86 ± 0.00	0.10 ± 0.00	7
1b-5-opx1*	53.89 ± 0.34	0.08 ± 0.01	5.25 ± 0.10	0.69 ± 0.02	5.59 ± 0.05	0.14 ± 0.02	31.94 ± 0.12	0.10 ± 0.02	0.01 ± 0.01	1.29 ± 0.02	0.11 ± 0.01	99.08 ± 0.30	0.85 ± 0.00	0.12 ± 0.00	6

N is the number of analyses

Uncertainties are reported as 1 standard deviation

*The grains used as RMs in the sample mount are marked with an asterisk

[a]FeO: all iron is treated as Fe^{2+}.

[b]Mg# is defined as MgO/(MgO+FeO)

[c]Cr# is defined as $Cr_2O_3/(Cr_2O_3+Al_2O_3)$

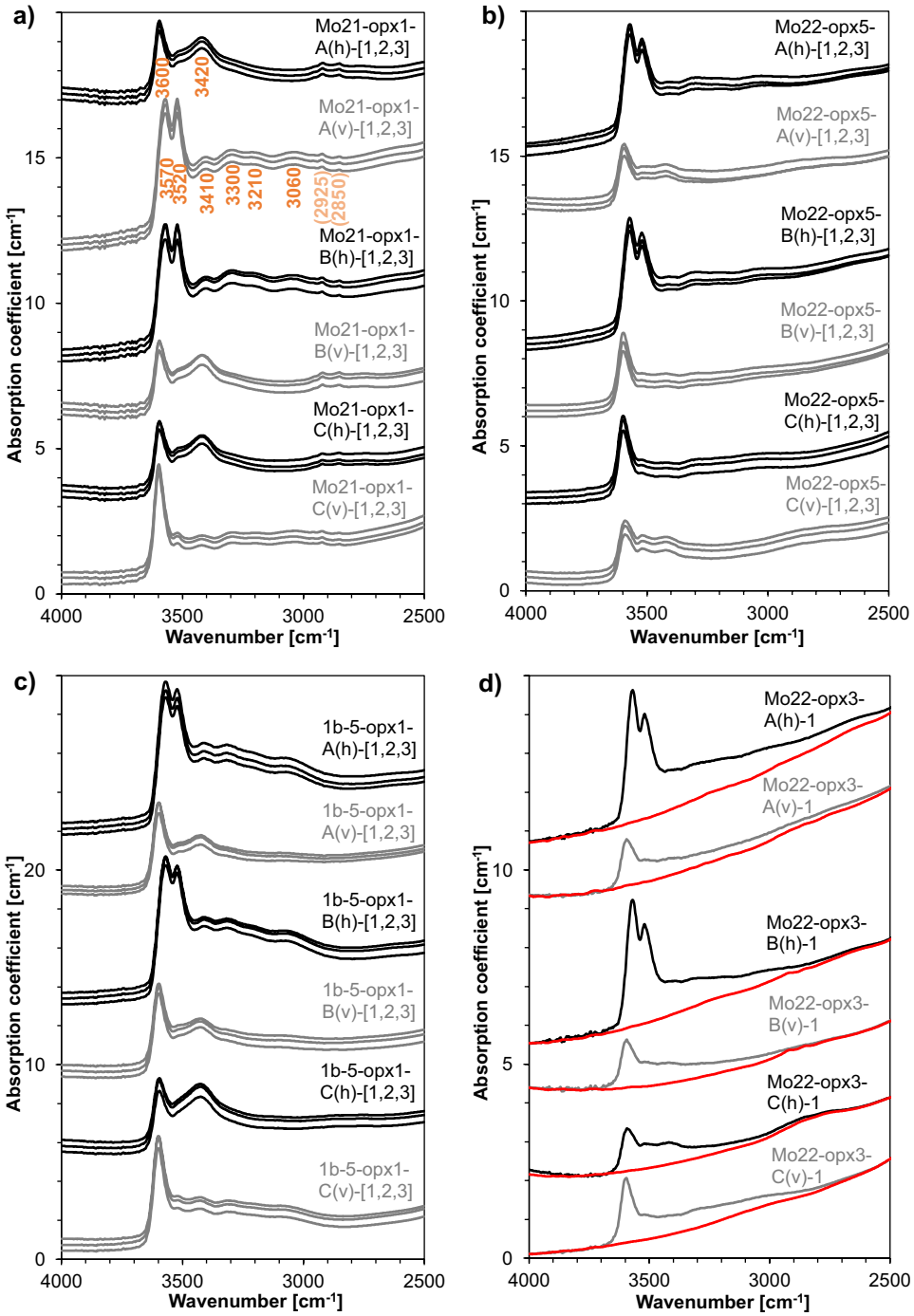

Fig. 2 Orthopyroxene FTIR spectra from three different spots (1, 2, 3) on the RMs that were used for the SIMS analyses of the abyssal peridotite orthopyroxene samples: **a**) Mo21-opx1, **b**) Mo22-opx5, **c**) 1b-5-opx1. Three mutually orthogonal grain orientations (A, B, C) collected in horizontal (h) and vertical (v) polarization mode were recorded for each spot. Absorption bands attributed to structural OH are labelled with the corresponding wavenumbers. Wavenumbers in brackets are ascribed to the epoxy introduced during the sample preparation. **d**) Data from dehydration experiment: one spectrum for each orientation of Mo22-opx3 is shown in black/grey before heat treatment and in red after heat treatment. All spectra are normalized to 1 cm thickness and have been shifted vertically for clarity

leading to a total of 18 spectra for one crystal. Importantly, the sets of six spectra representing the three different locations on the crystal contain the same OH bands of identical height in horizontal/vertical direction of the infrared polarizer, indicating that this material is homogenous in both its hydrogen content and in terms of the nature of the hydrogen molecular environment within the crystal. Thus, the H_2O concentrations of a single grain calculated for the three different locations are consistent.

Depending on crystal orientation, distinctive bands can be found in all samples around 3600, 3570, 3520, and 3420/3410 cm^{-1}, and less prominent bands around 3300, 3210, and 3060 cm^{-1}. These bands are ascribed to intrinsic OH in aluminous orthopyroxene (Beran and Zemann 1986; Skogby et al. 1990; Peslier et al. 2002; Stalder 2004). Pleochroism between the different orientations A, B, and C is variably strong since the individual grains are not oriented according to their crystallographic axes. Fig. 2d depicts

infrared spectra recorded both prior to and after dehydration of the grain Mo22-opx3. No hydrogen-bearing species are present in the dehydrated spectra. However, the different slopes and shapes of the spectra, depending on the crystal orientation, emphasize the problem of applying a proper background correction to each spectrum for calculating water contents.

Total H_2O concentrations of the reference orthopyroxenes measured by FTIR vary between 0 (dehydrated grain) and 249 ± 6 µg/g H_2O (Table 3). Within the range of uncertainty, multiple grains from one sample have the same or similar water contents: 148 ± 5 and 142 ± 4 µg/g H_2O for Mo21; 84 ± 4, 86 ± 3, 76 ± 5, 89 ± 5, 96 ± 3, and 77 ± 3 µg/g H_2O for Mo22; and 233 ± 8 and 227 ± 5 for E-K1. The good internal precision as indicated by low standard deviations is also notable.

As the range of orthopyroxene water contents from abyssal peridotites in former studies varies between 0 and 330 µg/g H_2O (Peslier et al. 2007; Warren and Hauri 2014; Hesse et al. 2015; Schmädicke et al. 2018) and we expect our samples from equivalent rocks to have similar contents, the selected reference minerals are well suited for use as SIMS calibration materials.

SIMS calibration

The subsequent SIMS determinations were calibrated using the reference orthopyroxenes that had been characterized by FTIR for their H_2O contents. These results are reported in Table 4. We concluded that a linear relationship exists between $H_2O_{(wt\%,\ FTIR)}$ vs. $(^1H^+/^{30}Si^+)_{SIMS} \times SiO_{2(wt\%,\ EPMA)}$. Therefore, the averaged measured $^1H^+/^{30}Si^+$ ratios are normalized by multiplication with SiO_2 (in wt%, EPMA data) and plotted against the H_2O concentrations determined by FTIR (Fig. 3). This relationship has a slope of 2.074×10^{-4} and a coefficient of determination of $R^2 = 0.97$. The limit of detection is <10 µg/g. In contrast to the FTIR values, where within the range of uncertainty, different orthopyroxene grains from the same sample record the same water content, the SIMS concentrations indicate that the water contents from different orthopyroxene grains of sample Mo22 are heterogenous. However, no differences between core and rim analyses could be detected in the two to five spots measured per grain, such that we assume intra-grain homogeneity.

Abyssal peridotite orthopyroxene samples

Major element composition

All orthopyroxenes from the abyssal peridotite samples are enstatites. The grains were found to be unzoned and homogenous concerning their major element contents. The SiO_2 content across the eight samples varies between 53.9 ± 0.4 wt% in sample HLY-102-D32 and 56.8 ± 0.4 wt% in sample PS59-249-Br4 (both from Gakkel Ridge), MgO between 32.5 ± 0.5 wt% in sample PS55-75-30 (Fram Strait) and 34.7 ± 0.4 wt% in sample PS59-249-Br4. Mg# ranges from 0.90 to 0.92, which is typical for mantle orthopyroxene. Cr# ranges from 0.08 (HLY-102-D32) to 0.20 (PS59-249-Br4) with Al_2O_3 contents from 1.66 ± 0.16 wt% (PS59-249-Br4) to 5.34 ± 0.31 wt% (HLY-102-D32) and Cr_2O_3 from 0.62 ± 0.08 wt% (PS59-249-Br4) to 0.96 ± 0.04 wt% (PS55-75-30) (Table 5). Thus, with the exception of samples PS59-249-Br4 and HLY-102-D32, the chromium contents of the abyssal peridotite orthopyroxenes are higher than in the RMs (0.21-0.69 wt% Cr_2O_3). The MgO contents of samples PS59-249-Br4, ODP109-670A-4R-1W, ODP125-0779A-26R-2W, and PS59-236-80-500-900 are also higher and aluminum contents of the same samples except for DSDP45-395-18R-1W-112 are lower than in the reference orthopyroxenes (31.4-32.9 wt% MgO, and 4.02-5.56 wt% Al_2O_3). All other elements were found to lie in the same range.

Water contents measured by SIMS

For eight out of twelve samples H_2O concentrations could successfully be quantified. The ODP304 orthopyroxenes from the Atlantis Massif and the ODP209 sample from the Mid-Atlantic Ridge are so highly altered that the indicated water contents lie far outside the calibrated range. Grain 1b-5-opx1 was used as the primary RM for the SIMS hydrogen determinations. Based on FTIR analyses this material has a hydrogen content of 249 ± 6 µg/g H_2O. On 13 determinations on 1b-5-opx1 a mean water content of 261 with a relative standard deviation of ± 8 % was obtained, which we believe is a reasonable estimate for the overall data quality at the higher end of our concentration range. Two other RMs, Mo21-opx1 with a nominal hydrogen content of 148 ± 5 µg/g H_2O and Mo22-opx5 with a nominal hydrogen content of 96 ± 3 µg/g H_2O via FTIR, were measured as SIMS quality control materials and to check for instrumental drift. These materials yielded concentration values of 125 ± 14 and 114 ± 6 µg/g H_2O, respectively (Table 6).

For reasons outlined above a calibration line forced through zero was deployed, plotting the averaged measured $^1H^+/^{30}Si^+$ ratios normalized by multiplication with SiO_2 (in wt%, EPMA data) against the H_2O concentrations determined by FTIR of the reference materials contained in the sample mount. This relation has a slope of 6.62×10^{-4} with a coefficient of determination of $R^2 = 0.99$ (Fig. 4). This calibration was used for the calculation of the water contents of the abyssal peridotite orthopyroxene samples.

The mean H_2O concentrations of the sample orthopyroxenes measured by SIMS range from 68 ± 7 µg/g in sample PS59-249-Br4 to 261 ± 11 µg/g in sample HLY-102-D32 (Table 6). Considering the 10 % standard deviation as a

Table 3 Integrated absorbance area normalized to 1 cm thickness and calculated H_2O concentration of the orthopyroxene grains used as reference materials in this study (total content and individual spectra) as determined by FTIR analysis

Reference orthopyroxene	Orientation/ polarization	Integrated absorbance area [cm^{-2}]	H_2O content [µg/g]	Orientation/ polarization	Integrated absorbance area [cm^{-2}]	H_2O content [µg/g]	Orientation/ polarization	Integrated absorbance area [cm^{-2}]	H_2O content [µg/g]	Total H_2O content [µg/g][a]
Mo21-opx1*	A(h)-1	510	35	B(h)-1	994	68	C(h)-1	482	33	148 ± 5
	A(h)-2	551	37	B(h)-2	1058	72	C(h)-2	527	36	
	A(h)-3	536	36	B(h)-3	998	68	C(h)-3	510	35	
	A(v)-1	1092	74	B(v)-1	476	32	C(v)-1	649	44	
	A(v)-2	1120	76	B(v)-2	525	36	C(v)-2	699	48	
	A(v)-3	1097	75	B(v)-3	499	34	C(v)-3	673	46	
Mo21-opx2	A(h)-1	512	35	B(h)-1	455	31	C(h)-1	616	42	142 ± 4
	A(h)-2	489	33	B(h)-2	484	33	C(h)-2	600	41	
	A(h)-3	532	36	B(h)-3	451	31				
	A(v)-1	1005	68	B(v)-1	600	41	C(v)-1	947	64	
	A(v)-2	1007	69	B(v)-2	630	43	C(v)-2	985	67	
	A(v)-3	1030	70	B(v)-3	607	41				
Mo22-opx1	A(h)-1	705	48	B(h)-1	702	48	C(h)-1	223	15	84 ± 4
	A(h)-2	657	45	B(h)-2	668	45	C(h)-2	251	17	
	A(h)-3	651	44	B(h)-3	697	47	C(h)-3	254	17	
	A(v)-1	250	17	B(v)-1	255	17	C(v)-1	386	26	
	A(v)-2	214	15	B(v)-2	232	16	C(v)-2	423	29	
	A(v)-3	204	14	B(v)-3	239	16	C(v)-3	407	28	
Mo22-opx2	A(h)-1	390	27	B(h)-1	288	20	C(h)-1	581	40	86 ± 3
	A(h)-2	392	27	B(h)-2	254	17	C(h)-2	606	41	
	A(h)-3	404	28	B(h)-3	264	18	C(h)-3	585	40	
	A(v)-1	393	27	B(v)-1	591	40	C(v)-1	288	20	
	A(v)-2	395	27	B(v)-2	531	36	C(v)-2	305	21	
	A(v)-3	424	29	B(v)-3	551	38	C(v)-3	292	20	
Mo22-opx3	A(h)-1	666	45	B(h)-1	572	39	C(h)-1	183	12	76 ± 5
	A(h)-2	757	52	B(h)-2	621	42	C(h)-2	207	14	
	A(h)-3	736	50	B(h)-3	627	43	C(h)-3	201	14	
	A(v)-1	194	13	B(v)-1	190	13	C(v)-1	269	18	
	A(v)-2	215	15	B(v)-2	216	15	C(v)-2	290	20	
	A(v)-3	223	15	B(v)-3	214	15	C(v)-3	285	19	

Table 3 (continued)

Reference orthopyroxene	Orientation/ polarization	Integrated absorbance area [cm^{-2}]	H_2O content [μg/g]	Orientation/ polarization	Integrated absorbance area [cm^{-2}]	H_2O content [μg/g]	Orientation/ polarization	Integrated absorbance area [cm^{-2}]	H_2O content [μg/g]	Total H_2O content [μg/g][a]
Mo22-opx4	A(h)-1	538	37	B(h)-1	772	53	C(h)-1	333	23	89 ± 5
	A(h)-2	568	39	B(h)-2	751	51	C(h)-2	358	24	
	A(h)-3	552	38	B(h)-3	716	49	C(h)-3	360	25	
	A(v)-1	282	19	B(v)-1	277	19	C(v)-1	356	24	
	A(v)-2	316	22	B(v)-2	276	19	C(v)-2	397	27	
	A(v)-3	299	20	B(v)-3	231	16	C(v)-3	405	28	
Mo22-opx5*	A(h)-1	745	51	B(h)-1	729	50	C(h)-1	383	26	96 ± 3
	A(h)-2	754	51	B(h)-2	710	48	C(h)-2	392	27	
	A(h)-3	736	50	B(h)-3	704	48	C(h)-3	365	25	
	A(v)-1	309	21	B(v)-1	374	25	C(v)-1	315	21	
	A(v)-2	316	22	B(v)-2	354	24	C(v)-2	320	22	
	A(v)-3	294	20	B(v)-3	335	23	C(v)-3	301	21	
Mo22-opx6	A(h)-1	508	35	B(h)-1	260	18	C(h)-1	573	39	77 ± 3
	A(h)-2	556	38	B(h)-2	257	17	C(h)-2	566	39	
	A(h)-3	532	36	B(h)-3	273	19	C(h)-3	577	39	
	A(v)-1	208	14	B(v)-1	445	30	C(v)-1	224	15	
	A(v)-2	236	16	B(v)-2	451	31	C(v)-2	225	15	
	A(v)-3	216	15	B(v)-3	470	32	C(v)-3	231	16	
Mo8531-opx1	A(h)-1	329	22	B(h)-1	362	25	C(h)-1	390	27	96 ± 3
	A(h)-2	312	21	B(h)-2	387	26	C(h)-2	404	27	
	A(h)-3	331	23	B(h)-3	336	23	C(h)-3	418	28	
	A(v)-1	590	40	B(v)-1	440	30	C(v)-1	700	48	
	A(v)-2	583	40	B(v)-2	458	31	C(v)-2	704	48	
	A(v)-3	594	40	B(v)-3	408	28	C(v)-3	682	46	
E-K1-opx1	A(h)-1	1466	100	B(h)-1	1484	101	C(h)-1	1037	71	233 ± 8
	A(h)-2	1462	100	B(h)-2	1496	102	C(h)-2	1056	72	
	A(h)-3	1457	99	B(h)-3	1319	90	C(h)-3	1068	73	
	A(v)-1	818	56	B(v)-1	979	67	C(v)-1	1143	78	
	A(v)-2	816	56	B(v)-2	930	63	C(v)-2	1140	78	
	A(v)-3	799	54	B(v)-3	871	59	C(v)-3	1183	81	

Table 3 (continued)

Reference orthopyroxene	Orientation/ polarization	Integrated absorbance area [cm^{-2}]	H_2O content [µg/g]	Orientation/ polarization	Integrated absorbance area [cm^{-2}]	H_2O content [µg/g]	Orientation/ polarization	Integrated absorbance area [cm^{-2}]	H_2O content [µg/g]	Total H_2O content [µg/g][a]
E-K1-opx3	A(h)-1	1499	102	B(h)-1	1497	102	C(h)-1	79	54	227 ± 5
	A(h)-2	1525	104	B(h)-2	1517	103	C(h)-2	793	54	
	A(h)-3	1507	103	B(h)-3	1514	103	C(h)-3	823	56	
							C(h)-4	777	53	
	A(v)-1	887	60	B(v)-1	896	61	C(v)-1	1047	71	
	A(v)-2	942	64	B(v)-2	924	63	C(v)-2	1067	73	
	A(v)-3	926	63	B(v)-3	912	62	C(v)-3	955	65	
							C(v)-4	1045	71	
1b-5-opx1*	A(h)-1	1916	130	B(h)-1	1789	122	C(h)-1	792	54	249 ± 6
	A(h)-2	1874	128	B(h)-2	1837	125	C(h)-2	820	56	
	A(h)-3	1816	124	B(h)-3	1842	125	C(h)-3	765	52	
	A(v)-1	944	64	B(v)-1	880	60	C(v)-1	1024	70	
	A(v)-2	916	62	B(v)-2	902	61	C(v)-2	1066	73	
	A(v)-3	870	59	B(v)-3	899	61	C(v)-3	1023	70	

*The grains used as RMs in the sample mount are marked with an asterisk

[a]Uncertainties are reported as 1 standard deviation of the "n" reported results

Table 4 SIMS data for the reference orthopyroxenes

Reference orthopyroxene	H_2O concentration by FTIR [μg/g][a]	Mean $^1H^+/^{30}Si^+$ counts measured	Mean $^1H^+/^{30}Si^+$ counts[x] SiO_2 content[wt.%]	H_2O concentration by SIMS [μg/g][a]
Mo21-opx1*	148 ± 5	5.35 x 10^{-4}	0.0294	137 ± 9
Mo21-opx2	142 ±4	4.81 x 10^{-4}	0.0265	122 ± 2
Mo22-opx1	84 ± 4	4.43 x 10^{-4}	0.0241	111 ± 1
Mo22-opx2	86 ± 3	2.79 x 10^{-4}	0.0151	68 ± 3
Mo22-opx3 (dehydrated)	0	2.35 x 10^{-5}	0.0013	1 ± 2
Mo22-opx4	89 ± 5	3.14 x 10^{-4}	0.0171	78 ± 4
Mo22-opx5*	96 ± 3	4.15 x 10^{-4}	0.0226	104 ± 2
Mo8531-opx1	96 ± 3	4.04 x 10^{-4}	0.0222	102 ± 4
E-K1-opx1	233 ± 8	9.98 x 10^{-4}	0.0541	256 ± 5
1b-5-opx1*	249 ± 6	9.45 x 10^{-4}	0.0509	241 ± 4

*The grains used as RMs in the sample mount are marked with an asterisk

[a]Uncertainties are reported as 1 standard deviation

benchmark, most of the samples show little or no heterogeneity in their H_2O contents. Also, no differences in water contents between core and rim analyses could be detected. The amounts of H_2O in the samples fall close to or within the range of contents of the RMs that were characterized by FTIR.

Water contents measured by FTIR

Several orthopyroxene fragments per sample were prepared for the FTIR analyses. The refined method of crushing the highly altered abyssal peridotite samples, however, failed to provide the desired data quality: in addition to secondary amphibole bands around 3690 cm^{-1} in many of the spectra (Skogby et al. 1990), absorption bands at ~2920 and ~2845 cm^{-1} interfered with our measurements (Fig. 5). We attribute these bands to traces of the epoxy that was used for the preparation of the less than mm-sized specimens and is possibly trapped in microfractures due to the crushing process (Grant et al. 2007; Tollan and Hermann 2019). We noted that this contamination extends as far as in the 3400 cm^{-1} region in our spectra, such that the contribution of the epoxy to the spectrum could not be assessed, effectively prohibiting the recovery of any meaningful information about the orthopyroxene H_2O content. Only for three grains from two samples (DSDP45-395-18R-1W-112 grains opx1 and opx4 and PS55-75-30 grain opx2) water contents could successfully be quantified. For two of these grains the water contents obtained by FTIR are significantly higher than the ones from the same samples obtained by SIMS: 100 ± 5 μg/g H_2O (SIMS) vs. 102 (+2 %) and 127 μg/g H_2O (+27 %; FTIR) for the two orthopyroxene fragments from DSDP45-395-18R-1W-112, and 206 ± 8 μg/g H_2O (SIMS) vs. 244 μg/g H_2O (+18 %; FTIR) for sample PS55-75-30 (Table 6). Whether there is a true difference between these SIMS and FTIR values or the discrepancy in these specific determinations is partially attributed to the epoxy cannot be evaluated at the present state of knowledge. However, the peridotites from both locations are highly altered, so generally one would expect the SIMS values to be higher if water-bearing alteration products were present in the analyzed sample volumes – as for example in the Atlantis Massif samples. As this is not the case, we conclude that for all other samples structurally incorporated water with little or no component derived from alteration processes was measured by SIMS.

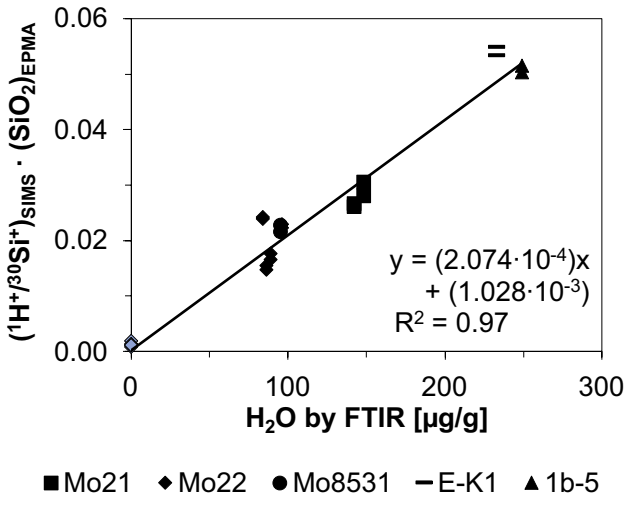

Fig. 3 SIMS calibration line produced by all RMs presented in this study. Mo22-opx3, the dehydrated RM, is shown in grey

Discussion

Water and major element contents

The orthopyroxene water contents in this study agree with H_2O concentrations of abyssal peridotite orthopyroxenes

Table 5 Averaged major element composition of the orthopyroxene samples from abyssal peridotites

Sample	SiO_2 [wt%]	TiO_2 [wt%]	Al_2O_3 [wt%]	Cr_2O_3 [wt%]	FeO* [wt%]	MnO [wt%]	MgO [wt%]	NiO [wt%]	ZnO [wt%]	CaO [wt%]	Na_2O [wt%]	Total [wt%]	Mg#[b]	Cr#[c]	N
DSDP45-395-18R-1W-112	55.34 ± 0.46	0.05 ± 0.01	3.42 ± 0.17	0.94 ± 0.05	6.10 ± 0.13	0.14 ± 0.02	32.60 ± 0.43	0.12 ±0.04	0.03 ±0.05	1.64 ± 0.49	0.01 ± 0.01	100.40 ± 0.57	0.91 ± 0.00	0.16 ± 0.01	11
PS59-249-Br4	56.83 ± 0.40	0.02 ± 0.01	1.66 ± 0.16	0.62 ± 0.08	5.06 ± 0.18	0.13 ± 0.02	34.71 ± 0.40	0.09 ±0.03	0.03 ± 0.03	1.14 ± 0.43	0.01 ± 0.01	100.31 ± 0.44	0.92 ± 0.00	0.20 ± 0.02	12
ODP109-670A-4R-1W	55.01 ± 0.46	0.05 ± 0.01	3.81 ± 0.09	0.83 ± 0.03	5.87 ± 0.11	0.13 ± 0.03	33.07 ± 0.38	0.10 ± 0.03	0.05 ± 0.06	1.51 ± 0.46	0.03 ± 0.01	100.47 ± 0.46	0.91 ± 0.00	0.13 ± 0.01	10
HLY-102-D32	53.95 ± 0.37	0.07 ± 0.01	5.34 ± 0.31	0.70 ± 0.06	6.12 ± 0.15	0.14 ± 0.02	32.58 ± 0.54	0.10 ± 0.03	0.03 ± 0.04	1.20 ± 0.37	0.02 ± 0.01	100.24 ± 0.41	0.90 ± 0.00	0.08 ± 0.00	12
ODP125-0779A-26R-2W	56.41 ± 0.21	0.01 ± 0.01	2.77 ± 0.13	0.74 ± 0.06	5.69 ± 0.16	0.14 ± 0.02	34.23 ± 0.31	0.08 ± 0.03	0.01 ± 0.02	0.70 ± 0.42	0.00 ± 0.01	100.79 ± 0.15	0.91 ± 0.00	0.15 ± 0.01	12
PS55-75-30	54.77 ± 0.78	0.11 ± 0.02	4.32 ± 0.08	0.96 ± 0.04	5.62 ± 0.20	0.14 ± 0.02	32.53 ± 0.49	0.11 ± 0.03	0.03 ± 0.03	1.52 ± 0.50	0.13 ± 0.06	100.23 ± 0.71	0.91 ± 0.00	0.13 ± 0.00	10
PS59-236-80-500-900	55.53 ± 0.45	0.02 ± 0.02	2.97 ± 0.39	0.86 ± 0.10	5.36 ± 0.14	0.15 ± 0.02	33.75 ± 0.51	0.10 ± 0.04	0.02 ± 0.02	1.49 ± 0.47	0.03 ± 0.02	100.27 ± 0.56	0.92 ± 0.00	0.16 ± 0.01	11
ME41/2-KD5-1	54.60 ± 0.45	0.04 ± 0.01	4.52 ± 0.20	0.87 ± 0.05	6.18 ± 0.14	0.16 ± 0.02	32.70 ± 0.27	0.10 ± 0.04	0.00 ± 0.00	1.46 ± 0.30	0.01 ± 0.01	100.63 ± 0.53	0.90 ± 0.00	0.11 ± 0.00	9

N is the number of analyses

Uncertainties are reported as 1 standard deviation

[a]FeO: all iron is treated as Fe^{2+}

[b]Mg# is defined as $MgO/(MgO+FeO)$

[c]Cr# is defined as $Cr_2O_3/(Cr_2O_3+Al_2O_3)$

Table 6 H_2O concentrations of the reference orthopyroxenes and the abyssal peridotite orthopyroxene samples measured by SIMS in comparison to the water contents obtained by FTIR

Reference orthopyroxene / sample	$^1H^+/^{30}Si^+$ counts measured	H_2O content [μg/g][a] by SIMS	N	H_2O content [μg/g][a] by FTIR
Mo21-opx1	0.0015	125 ± 14	17	148 ± 5
1b-5-opx1	0.0032	261 ± 8	13	249 ± 6
Mo22-opx5	0.0014	114 ± 6	11	96 ± 3
DSDP45-395-18R-1W-112	0.0012	100 ± 5	4	102 / 127
PS59-249-Br4	0.0008	68 ± 7	5	n.a.
ODP109-670A-4W-1W	0.0025	206 ± 7	4	n.a.
HLY-102-D32	0.0032	261 ± 11	4	n.a.
ODP125-U779A-26R-2W	0.0040	181 ± 9	4	n.a.
PS55-75-30	0.0025	206 ± 8	5	244
PS59-236-80-500-900	0.0012	98 ± 9	4	n.a.
ME41/2-KD5-1	0.0020	161 ± 6	5	n.a.

N is the number of analyses

n.a. indicates that quantification of FTIR water contents was not possible

[a]Uncertainties are reported as 1 standard deviation

published in other studies. Our DSDP45-395-18R-1W-112 and ODP109-670A-4R-1W samples, both from the 23°N region at the Mid-Atlantic Ridge have SIMS water contents of 100 ± 5 μg/g and 206 ± 7 μg/g, respectively. This is a wide range, however, the higher value is consistent with orthopyroxene data from ODP Leg 153 (23°20'N, Kane Transform, Mid-Atlantic Ridge), which contain 220–323 wt. ppm H_2O measured by FTIR (Schmädicke et al. 2018). Leg 209 samples (15°39' N at the MAR) in the same study range from 121–231 wt. ppm H_2O. Unfortunately, we were not able to obtain a water content for our ODP209-1272A-26R-1W-60-65 sample, as the grain was too highly altered. The sample ME41/2-KD5-1 orthopyroxene from the Southern Atlantic Ocean contains 161 ± 6 μg/g H_2O.

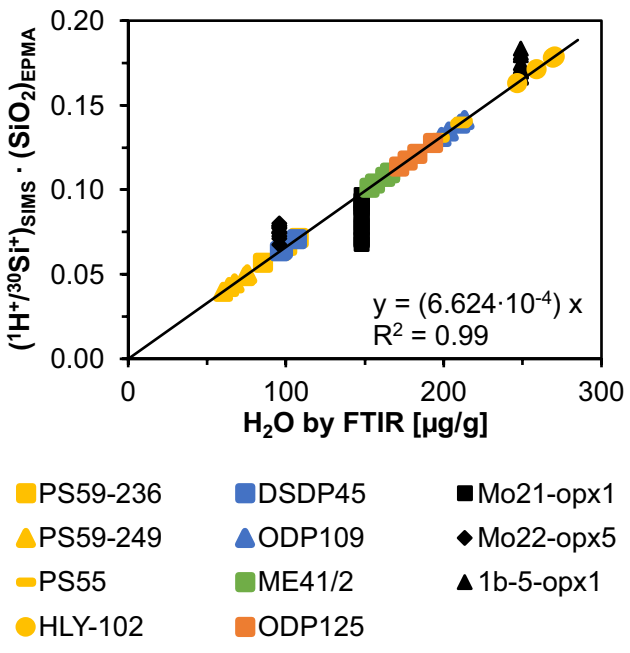

Fig. 4 SIMS calibration line for the analyses of the abyssal peridotite orthopyroxene samples produced by RMs Mo22-opx5, Mo21-opx1, and 1b-5-opx1 containing 96, 148, and 249 μg/g H_2O, respectively, based on FTIR (black symbols). Water contents of the samples (colored symbols) are calculated using this calibration. Yellow symbols are used for the Arctic samples, blue for the Atlantic samples, green for the South Atlantic sample and orange for the Pacific sample

The highest water content in this study is detected in the HLY-102-D32 sample from Gakkel Ridge, which contains 261 ± 11 μg/g H_2O. This is somewhat surprising since Peslier et al. (2007) measured distinctively lower water concentrations of 25–60 wt. ppm by FTIR for enstatites of PS66-238 samples dredged at the Gakkel Ridge. The orthopyroxene grains from samples PS59-249-Br4 and PS59-236-80-500-900 in this study, also from Gakkel Ridge, contain significantly less water: 68 ± 7 μg/g and 98 ± 9 μg/g, respectively. Nonetheless, the second value is still higher than in the Peslier et al. (2007) study. Warren and Hauri (2014) also examined two orthopyroxenes from Gakkel Ridge (HLY0102-4081 and PS59-235-17) in their SIMS study, which contain 99 ± 10 and 145 ± 18 wt. ppm H_2O, respectively. These water contents are consistent with our PS59-236-80-500-900 sample. For the orthopyroxene grain from sample PS55-75 from the Arctic Ocean, another very high H_2O concentration of 206 ± 8 μg/g was determined.

The ODP125-0779A-26R-2W orthopyroxene from the Izu-Bonin-Mariana forearc region in this study contains 181 ± 9 μg/g H_2O. A recent study by Gose and Schmädicke (2021) also investigated ODP Leg 125 and measured comparable orthopyroxene water contents between 122 and 363

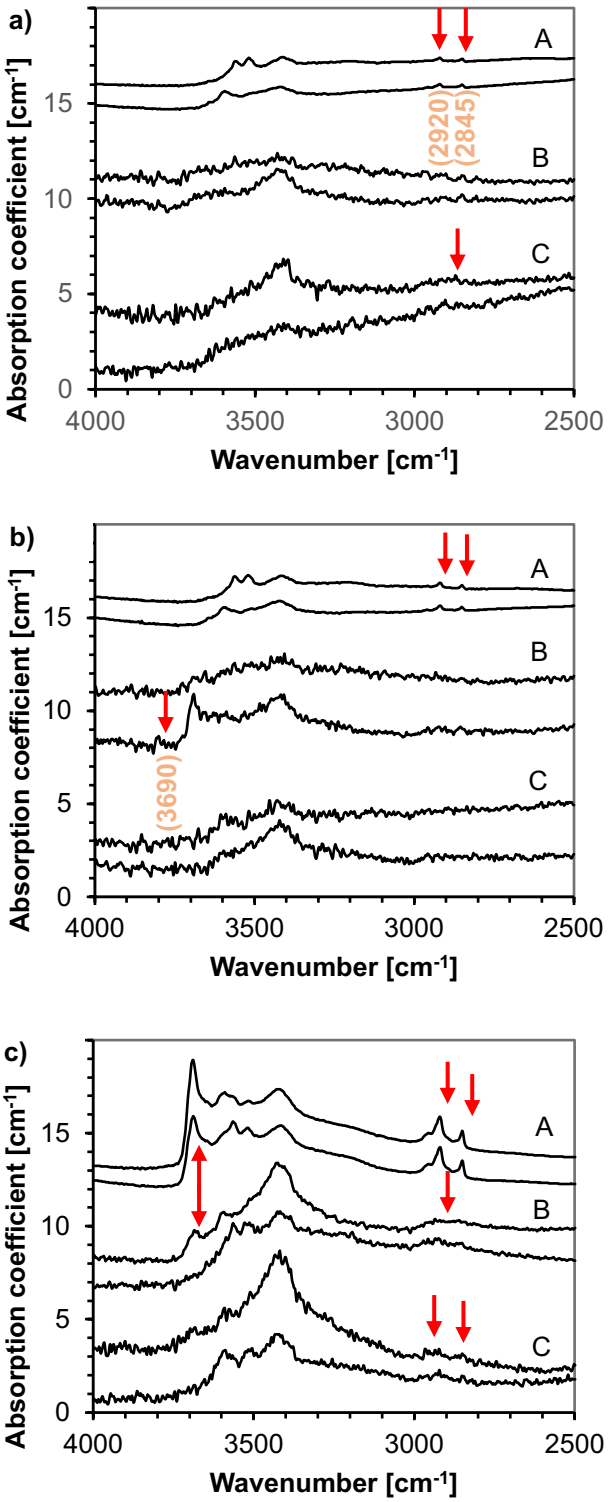

Fig. 5 FTIR spectra from three abyssal peridotite orthopyroxene grain fragments: **a**) DSDP45-opx1 (102 µg/g H_2O), **b**) DSDP45-opx4 (127 µg/g H_2O), and **c**) PS55-75-opx2 (244 µg/g H_2O) that could successfully be quantified. Spectra for each orientation A, B, and C in horizontal and vertical polarization are shown. The arrows indicate bands attributed to amphibole (3690 cm^{-1}) and residual traces of epoxy (2920 and 2845 cm^{-1}). The spectra are normalized to 1 cm thickness and shifted vertically for clarity. Depending on crystal quality, apertures smaller than 50x50 $µm^2$ were used which resulted in less smooth spectra

wt. ppm H_2O by FTIR (average 215 wt. ppm H_2O) at Conical seamount.

In contrast to experimental data on doped crystals where correlations of water contents with major elements are evident (Rauch and Keppler 2002; Stalder and Skogby 2002; Stalder 2004; Stalder et al. 2005), correlations in natural samples are less obvious due to their greater chemical complexity. However, several studies on natural upper mantle orthopyroxene have found well-defined correlations between the mineral's water content and its Al_2O_3, FeO, and/or MgO contents (Peslier and Bizimis 2015; Kilgore et al. 2018; Schmädicke et al. 2018; Schaffer et al. 2019; Ashley et al. 2020). The present set of samples also indicates that major element composition and SIMS determined water contents are related. Our abyssal peridotite orthopyroxene samples from diverse locations cover a broad range of Mg# and Cr# (Fig. 6a). In particular Cr# (Fig. 6c) and Al_2O_3 (Fig. 6d) correlate well with the H_2O contents measured by SIMS (r = -0.89 and 0.80, respectively). Correlation coefficients with TiO_2 (Fig. 6b), FeO (Fig. 6f) and MgO are 0.59, 0.56, and -0.55, respectively. Other major elements do not seem to be related to the amount of structural water.

SIMS versus FTIR

Once a calibration and analytical routine have been established, SIMS offers the advantages of being a rapid method for quantifying total hydrogen contents with the potential of analyzing targeted samples in the low nanogram mass range. In the case of abyssal peridotite, SIMS also has the major advantage of much simpler sample preparation requirements as compared to FTIR, because the latter requires the preparation of crystals in three orientations. On the other hand, a significant challenge of the SIMS technology is the need for well-characterized, matrix-matched reference materials, which ideally include a blank material. Another aspect is the need to assure exceptionally good vacuum quality in the analysis chamber, as the residual H_2O and H_2 in the chamber can be a significant source of background due to molecules adsorbed at the analysis location during the course of data acquisition. For our samples with water contents of (several) hundred µg/g H_2O a possible hydrogen background of a few µg/g H_2O was not a major concern. Koga et al. (2003) report hydrogen counts of tens of ions per second, corresponding to a blank of 2-4 µg/g H_2O, which is similar to what can be achieved with FTIR. An FTIR detection limit below ~1 µg/g H_2O is very challenging because of issues related to the optical quality of the sample, possible biases introduced by the various calibration strategies, and the method of baseline correction (Mosenfelder and Rossman 2013; Kumamoto et al. 2017). The main disadvantage of FTIR is that depending on the method (polarized measurements in three orthogonal orientations vs. non-polarized/statistical

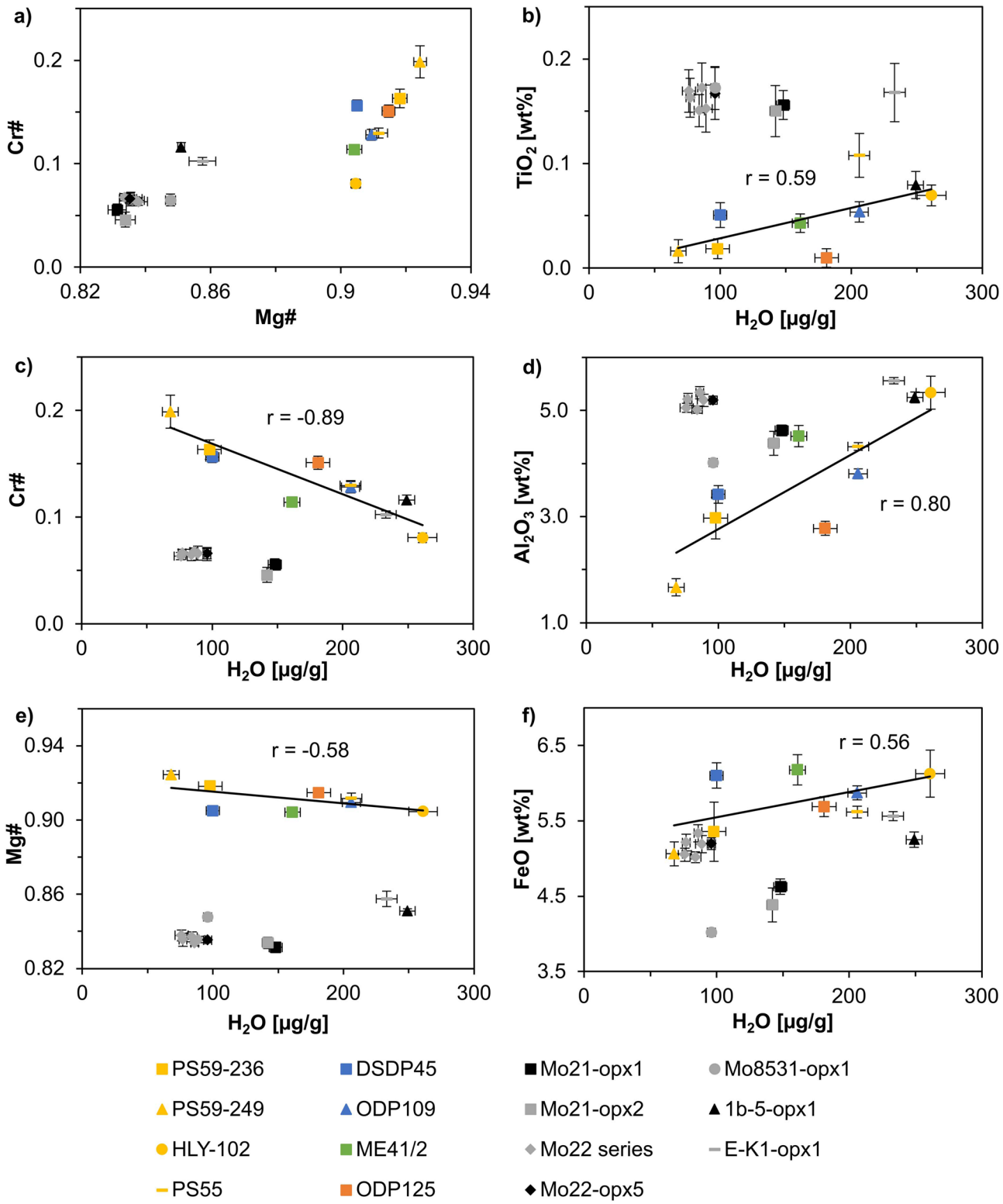

Fig. 6 SIMS water contents as a function of major element composition determined from EPMA analyses for our set of abyssal peridotite orthopyroxene samples (colored symbols) and the new RMs in this study (black and grey symbols). a) Mg# versus Cr#, b) H O versus TiO , c) H O versus Cr#, d) H O versus Al O , e) H O versus Mg#, f) H O versus FeO. Black symbols are assigned to the three RMs used for the SIMS calibration of our sample analyses. All other RMs are shown in grey. The error bars correspond to 1 standard deviation

measurements in only one orientation) sample preparation can easily become very time-intensive or even impossible, particularly for small or poor-quality samples such as abyssal peridotite, which usually contains only few suitable grains on thin section scale.

As spatial resolution is higher, SIMS is a reliable technique for detecting compositional zoning within a crystal. Depending on the quality of the crystal, the volume analyzed by FTIR can easily become very large (150x150x1660 μm^3 as in the case of the largest RM in this study, but with typical volumes of 50x50x250 μm^3 for abyssal peridotite orthopyroxene grains), and one only gets an averaged value for the water content integrated over this volume. The sample volume of SIMS is smaller, often less than 10x10x1 μm^3, such that zonation due to diffusional water loss/gain or compositional variation resulting from differing crystal growth events can effectively be identified and quantified.

While SIMS records total water contents, FTIR provides the significant advantage of also yielding information about hydrogen speciation, i.e. the type of substitution mechanisms, as well as possible alteration products, hydrous fluid inclusions, and secondary phases. This additional information can be essential for understanding the geological history of a sample, including such issues as thermobarometric conditions at the time of hydrogen incorporation, the assessment of redox conditions, and bulk dewatering trends brought about by high grade regional metamorphism.

Conclusion

This study has demonstrated that when investigating pyroxenes from highly altered oceanic peridotite samples, SIMS offers significant advantages for quantifying intracrystalline H_2O contents. The SIMS sampling volume is much smaller than that offered by FTIR, allowing cracks and zones of alteration to be avoided. When SIMS analysis targets are selected carefully using optical and/or SEM imaging, water contents un-affected by alteration or inclusions can be obtained by SIMS. We observed that the water contents calculated from the SIMS analyses, although about 20% lower than the corresponding FTIR values for two samples, are similar within the range of uncertainty of the two methods, which indicates that the SIMS results do correspond to crystal bound, structural OH with little or no component derived from younger alteration processes. If this were not the case, water contents from differing localities should expectedly be much higher and scatter over a wide range of values, which is not seen in the present SIMS data.

As FTIR has the important strength of being able to distinguish between the different hydrogen species, which is needed in order to get a better understanding of the evolution of the water contents of such rocks, we suggest a combination of both methods, especially for "difficult" samples such as abyssal peridotites. We conclude that the optimal strategy combines both methods by first analyzing an individual grain by FTIR to get an overview of alteration and water content and then measure the same grain at multiple, carefully targeted locations using SIMS from which the homogeneity of the H_2O distribution can be assessed. This two-step approach provides the possibility of gaining a complete picture of the evolution of such complex materials such that implications about the geological history of the rocks can be made.

Equally important, an additional benefit of this project is that it has resulted in a set of natural reference orthopyroxenes which have been carefully cross-calibrated between FTIR (used to define the absolute hydrogen abundances) and SIMS (used to confirm micron-scale homogeneity of the hydrogen distribution). These eleven reference minerals yielding reproducible data and a SIMS limit of detection of <10 µg/g for H_2O in orthopyroxene are described in detail in this manuscript.

The water contents of orthopyroxenes from a suite of highly serpentinized abyssal peridotites from the Atlantic and Arctic Ridges as well as from the Izu-Bonin-Mariana forearc region, being difficult to impossible to analyze by FTIR, were measured using these reference orthopyroxenes according to the outlined strategy. The eight samples determined via SIMS gave water contents ranging between 68 ± 7 and 261 ± 11 µg/g H_2O, which is consistent with literature data for abyssal peridotites (see Gose and Schmädicke 2021; and references therein). All samples and reference orthopyroxenes have homogenous water concentrations at grain scale, such that no signs of water gain or loss could be detected for either tectonically exhumed peridotites or mantle xenoliths.

Acknowledgements Gudrun Witt-Eickschen and Heinz-Günter Stosch are thanked for the Eifel and Mongolian samples, respectively. Marcel Regelous and Christoph Weinzierl generously provided abyssal peridotite samples. We thank Uwe Dittmann for help preparing the SIMS sample mounts and Frédéric Couffignal for his outstanding support in the SIMS laboratory. Roland Stalder at the University of Innsbruck is thanked for assistance with the FTIR spectrometer. The paper benefitted from critical, yet constructive and very helpful reviews by an anonymous reviewer and by Anne Peslier, and from comments from Associate Editor Anton Beran, whom is thanked for his patience in the editorial handling. Funding of this research was provided by the Deutsche Forschungsgemeinschaft (grant number: Schm1039/12-1) and the "Bavarian Equal Opportunities Sponsorship - Realisierung von Chancengleichheit von Frauen in Forschung und Lehre (FFL) - Realization Equal Opportunities for Women in Research and Teaching", which are both gratefully acknowledged.

Funding Open Access funding enabled and organized by Projekt DEAL.

References

Ashley AW, Bizimis M, Peslier AH, Jackson M, Konter JG (2020) Metasomatism and hydration of the oceanic lithosphere: A case study of peridotite xenoliths from Samoa. J Petrol 61(2):egaa028

Aubaud C, Withers AC, Hirschmann MM, Guan Y, Leshin LA, Mackwell SJ, Bell DR (2007) Intercalibration of FTIR and SIMS for hydrogen measurements in glasses and nominally anhydrous minerals. Am Mineral 92:811–828

Azevedo-Vannson S, France L, Ingrin J, Chazot G (2021) Mantle metasomatic influence on water contents in continental lithosphere: New constraints from garnet pyroxenite xenoliths (France & Cameroon volcanic provinces). Chem Geol 575:120257

Bell DR, Ihinger PD, Rossman GR (1995) Quantitative analysis of trace OH in garnet and pyroxenes. Am Mineral 80:465–474

Bell DR, Rossman GR (1992) Water in Earth's Mantle: The role of nominally anhydrous minerals. Science 255:1391–1397

Bell DR, Rossman GR, Maldener J, Endisch D, Rauch F (2003) Hydroxide in olivine: A quantitative determination of the absolute amount and calibration of the IR spectrum. J Geophys Res 108(B2):2105

Beran A, Zemann J (1986) The pleochroism of a gem-quality enstatite in the region of the OH stretching frequency, with a stereochemical interpretation. TMPM Tschermaks Mineral und Petrogr Mitteilungen 35:19–25

Demouchy S, Jacobsen SD, Gaillard F, Stem CR (2006) Rapid magma ascent recorded by water diffusion profiles in mantle olivine. Geology 34:429–432

Demouchy S, Tommasi A, Barou F, Mainprice D, Cordier P (2012) Deformation of olivine in torsion under hydrous conditions. Phys Earth Planet Inter 202–203:56–70

Denis CMM, Demouchy S, Alard O (2018) Heterogeneous hydrogen distribution in orthopyroxene from veined mantle peridotite (San Carlos, Arizona): Impact of melt-rock interactions. Lithos 302–303:298–311

Denis CMM, Demouchy S, Shaw CSJ (2013) Evidence of dehydration in peridotites from Eifel Volcanic Field and estimates of the rate of magma ascent. J Volcanol Geotherm Res 258:85–99

Gose J, Schmädicke E (2021) Water in the supra-subduction-zone mantle of the Mariana-Izu-Bonin forearc: constraints from peridotitic orthopyroxene. Geochem Geophys Geosyst 22(4):e2020GC009586

Gose J, Schmädicke E, Beran A (2009) Water in enstatite from Mid-Atlantic Ridge peridotite: Evidence for the water content of suboceanic mantle? Geology 37:543–546

Gose J, Schmädicke E, Stalder R (2011) Water in mantle orthopyroxene – no visible change in defect water during serpentinization. Eur J Mineral 23:529–536

Grant KJ, Ingrin J, Lorand JP, Dumas P (2007) Water partitioning between mantle minerals from peridotite xenoliths. Contrib to Mineral Petrol 154:15–34

Hao Y, Xia Q, Li Q, Chen H, Feng M (2014) Partial melting control of water contents in the Cenozoic lithospheric mantle of the Cathaysia block of South China. Chem Geol 380:7–19

Hauri EH, Shaw AM, Wang J, Dixon JE, King PL, Mandeville C (2006) Matrix effects in hydrogen isotope analysis of silicate glasses by SIMS. Chem Geol 235:352–365

Hesse KT, Gose J, Stalder R, Schmädicke E (2015) Water in orthopyroxene from abyssal spinel peridotites of the East Pacific Rise (ODP Leg 147: Hess Deep). Lithos 232:23–34

Hirschmann MM, Aubaud C, Withers AC (2005) Storage capacity of H2O in nominally anhydrous minerals in the upper mantle. Earth Planet Sci Lett 236:167–181

Hirth G, Kohlstedt DL (1996) Water in the oceanic upper mantle: implications for rheology, melt extraction and the evolution of the lithosphere. Earth Planet Sci Lett 144:93–108

Kilgore ML, Peslier AH, Brandon AD, Lamb WM (2018) Water and Oxygen Fugacity in the Lithospheric Mantle Wedge beneath the Northern Canadian Cordillera (Alligator Lake). Geochemistry, Geophys Geosystems 19:3844–3869

Koga K, Hauri EH, Hirschmann M, Bell DR (2003) Hydrogen concentration analyses using SIMS and FTIR: Comparison and calibration for nominally anhydrous minerals. Geochemistry, Geophys Geosystems 4(2):1019

Kohn SC (2006) Structural Studies of OH in nominally anhydrous minerals using NMR. Rev Mineral Geochem 62:53–66

Kumamoto KM, Warren JM, Hauri EH (2017) New SIMS reference materials for measuring water in upper mantle minerals. Am Mineral 102:537–547

Libowitzky E, Beran A (2004) IR spectroscopic characterization of hydrous species in minerals. In: Beran A, Libowitzky E (eds) Spectroscopic Methods in Mineralogy. EMU Notes Mineral 6, Budapest, pp 227–279

Libowitzky E, Beran A (2006) The structure of hydrous species in nominally anhydrous minerals: Information from polarized IR spectroscopy. In: Keppler H, Smyth JR (eds) Water in Nominally Anhydrous Minerals. Rev Mineral Geochem, vol 62. Mineral Soc Am, Chantilly, pp 29–52

Libowitzky E, Rossman GR (1996) Principles of quantitative absorbance measurements in anisotropic crystals. Phys Chem Miner 23:319–327

Mackwell SJ, Kohlstedt DL (1990) Diffusion of hydrogen in olivine: implications for water in the mantle. J Geophys Res 95:5079–5088

Mosenfelder JL, Rossman GR (2013) Analysis of hydrogen and fluorine in pyroxenes: I. Orthopyroxene. Am Mineral 98:1026–1041

Mosenfelder JL, Le Voyer M, Rossman GR et al (2011) Analysis of hydrogen in olivine by SIMS: Evaluation of standards and protocol. Am Mineral 96:1725–1741

Peslier AH (2010) A review of water contents of nominally anhydrous natural minerals in the mantles of Earth, Mars and the Moon. J Volcanol Geotherm Res 197:239–258

Peslier AH, Bizimis M (2015) Water in Hawaiian peridotite minerals: A case for a dry metasomatized oceanic mantle lithosphere. Geochemistry, Geophys Geosystems 16:1211–1232

Peslier AH, Luhr JF (2006) Hydrogen loss from olivines in mantle xenoliths from Simcoe (USA) and Mexico: Mafic alkalic magma ascent rates and water budget of the sub-continental lithosphere. Earth Planet Sci Lett 242:302–319

Peslier AH, Luhr JF, Post J (2002) Low water contents in pyroxenes from spinel-peridotites of the oxidized, sub-arc mantle wedge. Earth Planet Sci Lett 201:69–86

Peslier AH, Snow JE, Hellebrand E, von der Handt A (2007) Low water contents in minerals from Gakkel ridge abyssal peridotites, Arctic Ocean. In: Goldschmidt Conference Abstracts 779, Cologne, Germany

Rauch H, Keppler M (2000) Water solubility in nominally anhydrous minerals measured by FTIR and 1 H MAS NMR: the effect of sample preparation. Phys Chem Miner 27:371–376

Rauch M, Keppler H (2002) Water solubility in orthopyroxene. Contrib to Mineral Petrol 143:525–536

Regelous M, Weinzierl CG, Haase KM (2016) Controls on melting at spreading ridges from correlated abyssal peridotite - mid-ocean ridge basalt compositions. Earth Planet Sci Lett 449:1–11

Rossman GR (1996) Studies of OH in nominally anhydrous minerals. Phys Chem Miner 23:299–304

Rossman GR (2006) Analytical methods for measuring water in nominally anhydrous minerals. Rev Mineral Geochem 62:1–28

Schaffer LA, Peslier AH, Brandon AD, Bizimis M, Gibler R, Norman M, Harvey J (2019) Effects of melting, subduction-related metasomatism, and sub-solidus equilibration on the distribution of water contents in the mantle beneath the Rio Grande Rift. Geochim Cosmochim Acta 266:351–381

Schmädicke E, Gose J, Stalder R (2018) Water in abyssal peridotite: Why are melt-depleted rocks so water rich? Geochemistry, Geophys Geosystems 19:1824–1843

Schmädicke E, Gose J, Will TM (2011) Heterogeneous mantle underneath the North Atlantic: Evidence from water in orthopyroxene, mineral composition and equilibrium conditions of spinel peridotite from different locations at the Mid-Atlantic Ridge. Lithos 125:308–320

Schmädicke E, Gose J, Witt-Eickschen G, Brätz H (2013) Olivine from spinel peridotite xenoliths: Hydroxyl incorporation and mineral composition. Am Mineral 98:1870–1880

Sheng Y, Gong B, Li W, Xia M (2016) Methodological progress in trace amounts of structural water in nominally anhydrous minerals. Sci China 59:901–909

Skogby H, Bell DR, Rossman GR (1990) Hydroxide in pyroxene: Variations in the natural environment. Am Mineral 75:764–774

Stalder R (2004) Influence of Fe, Cr and Al on hydrogen incorporation in orthopyroxene. Eur J Mineral 16:703–711

Stalder R, Klemme S, Ludwig T, Skogby H (2005) Hydrogen incorporation in orthopyroxene: interaction of different trivalent cations. Contrib to Mineral Petrol 150:473–485

Stalder R, Skogby H (2002) Hydrogen incorporation in enstatite. Eur J Mineral 14:1139–1144

Stosch H-G, Seck HA (1980) Geochemistry and mineralogy of two spinel peridotite suites from Dreiser Weiher, West Germany. Geochim Cosmochim Acta 44:457–470

Tian ZZ, Liu J, Xia Q-K, Ingrin J, Hao Y-T, Depecker C (2016) Water concentration profiles in natural mantle orthopyroxenes: A geochronometer for long annealing of xenoliths within magma. Geology 44:87–90

Tielke JA, Zimmerman ME, Kohlstedt DL (2017) Hydrolytic weakening in olivine single crystals. J Geophys Res Solid Earth 122:3465–3479

Tollan P, Hermann J (2019) Arc magmas oxidized by water dissociation and hydrogen incorporation in orthopyroxene. Nat Geosci 12:667–671

Warren JM, Hauri EH (2014) Pyroxenes as tracers of mantle water variations. J Geophys Res Solid Earth 119:1851–1881

Withers AC, Bureau H, Raepsaet C, Hirschmann MM (2012) Calibration of infrared spectroscopy by elastic recoil detection analysis of H in synthetic olivine. Chem Geol 334:92–98